Published in final edited form as:
J Magn Reson Imaging. 2010 December ; 32(6): 1353–1369. doi:10.1002/jmri.22383.

Recent technological and application developments in computed tomography and magnetic resonance imaging for improved pulmonary nodule detection and lung cancer staging

Jessica C. Sieren, Ph.D.[1,4], **Yoshiharu Ohno, M.D., Ph.D.**[2], **Hisanobu Koyama, M.D., Ph.D.**[2], **Kazuro Sugimura, M.D.**[2], and **Geoffrey McLennan, M.D., Ph.D.**[1,3,4]

[1] Department of Internal Medicine, University of Iowa, 200 Hawkins Drive, Iowa City, Iowa, USA 52242

[2] Department of Radiology, Kobe University Graduate School of Medicine, 7-5-2 Kusunoki-cho, Chuo-ku, Kobe, 650-0017, Japan

[3] Department of Radiology, University of Iowa, 200 Hawkins Drive, Iowa City, Iowa, USA 52242

[4]Department of Biomedical Engineering, University of Iowa, 200 Hawkins Drive, Iowa City, Iowa, USA 52242

Abstract

This review compares the emerging technologies and approaches in the application of magnetic resonance (MR) and computed tomography (CT) imaging for the assessment of pulmonary nodules and staging of malignant findings. Included in this review is a brief definition of pulmonary nodules and an introduction to the challenges faced. We have highlighted the current status of both MR and CT for the early detection of lung nodules. Developments are detailed in this review for the management of pulmonary nodules using advanced imaging, including; dynamic imaging studies, dual energy CT, computer aided detection and diagnosis, and imaging assisted nodule biopsy approaches which have improved lung nodule detection and diagnosis rates. Recent advancements linking in-vivo imaging to corresponding histological pathology are also highlighted. In-vivo imaging plays a pivotal role in the clinical staging of pulmonary nodules through TNM assessment. While CT and PET/CT are currently the most commonly clinically employed modalities for pulmonary nodule staging, studies are presented which highlight the augmentative potential of MR.

Keywords

Computed tomography; magnetic resonance; tumor; functional imaging; visualization; staging

Introduction

Lung cancer remains a challenging disease to effectively identify, diagnose and treat as is reflected by the 5 year survival rate which remains similar to that of fifteen years ago at

Corresponding Author: Jessica Sieren, 344 MRC, University of Iowa, Iowa City, IA 52242, Tel: (319) 384-1024, Fax: (319) 384-1023, jessica-sieren@uiowa.edu.

Conflict of Interest: Dr McLennan is part owner of VIDA Diagnostics.

Dr Ohno and Dr Sugimura have research grants from Toshiba Corporations, Philips Healthcare, Bayer AG, DAIICHI SANKYO group and Eisai Co, Ltd.

13%. Lung cancer frequently manifests as a peripheral lung nodule or mass. Radiologically identified lesions in the lung that are less than 30mm in diameter are defined as pulmonary nodules while those greater than 30mm are termed masses (1). Both pulmonary nodules and masses present specific challenges in the evaluation of suspected lung cancer, however the greatest impact of x-ray computed tomography (CT) and magnetic resonance (MR) imaging developments have been on the detection and characterization of pulmonary nodules. Hence the scope of this review will focus on the recent advances in CT and MR imaging of pulmonary nodules and lung cancer staging, highlighting the respective strengths and weaknesses of these modalities.

CXR is the most widely utilized modality for pulmonary abnormalities and disease screening, although sonography has been utilized for limited situation in the chest. In addition, PET or PET/CT with 2-Deoxy-2-[18F]fluoro-D-Glucose (FDG) is currently widely utilized for differentiation of malignant lesions from benign lesions, staging of malignant tumors, and assessment of therapeutic effects after conservative therapy. The value of CT and MR for depicting structural anatomy is widely appreciated and applied clinically to non-invasively identify abnormalities and/or disease. Recent developments of imaging techniques and processing have expanded the potential of these modalities to include combined structure and function. Recent exciting work for the detection, monitoring, characterization and staging of pulmonary cancer nodules using imaging both CT and MR modalities will be summarized in this review.

While the overall objective of using imaging, as a method of improving patient care, is the same for both modalities, and the present performance of both modalities for pulmonary applications differs not only due to specific challenges to be faced but also due to the amount of development that has been invested in their lung imaging capacities. X-ray imaging of which CT is the volumetric derivative, has a relatively long history in the diagnosis and treatment planning of pulmonary disease, including pulmonary nodules, while MR imaging has been developed more recently. Significant challenges in MR signal acquisition in the lung still exist, caused by low proton density, very short T2* values and inhomogenity of magnetic field in the lung, and cardiac and respiratory motion artifacts. Due to these challenges the application of MR imaging for lung nodule analysis has been a relatively recent development, however the growth in this field has been rapid.

Recent technological advances in CT and MR have been compelling. In CT, developments in acquisition have led to dose reduction through techniques such as iterative reconstruction and have also facilitated four dimensional imaging (3D plus time). The complex utilization of the generated data has resulted in virtual bronchoscopy for guided biopsy and computer assisted nodule detection and characterization. In MR, advanced protocol developments have revealed significant potential for pulmonary nodule assessment as well as pulmonary functional imaging in the last decade. Future efforts are required to maximize the benefits of each system through effective integration of both modalities in pulmonary nodule applications.

Pulmonary Lung Nodules

A pulmonary nodule is radiologically defined in two dimensions (2D) as a roughly round, intraparenchymal lung lesion that is less than 30 mm in diameter and is not associated with atelectasis or adenopathy (1). While one in 500 x-ray chest radiographs (CXRs) shows a lung nodule, 90% of these nodules are incidental radiologic findings, detected accidentally on CXRs obtained for unrelated diagnostic workups. More than 150,000 patients per year in United States present their physicians with the diagnostic dilemma of a pulmonary nodule. This number has increased even further due to incidental findings of lung nodules on chest

CT (1-3). Patients with the best prognosis are those with stage IA disease, hence timely and accurate detection and diagnosis of the etiology of pulmonary nodules including lung metastasis are therefore essential to potentially cure patients with malignancy.

Early Detection of Pulmonary Nodules with CT and MR Imaging

The first clinical application of CT occurred in 1971, capturing a brain lesion, and applications in the lung were boosted with the1980's development of helical CT and faster acquisition times (4). The latest commercially released multi-detector computed tomography (MDCT) systems are increasingly complex, with 128 or more detectors and temporal resolutions in the order of 75 ms; a complete thorax scan can be acquired in less than one second. The exceptionally rapid acquisition time of MDCT benefits patients by removing the need for breath-holds or gating and is also advantageous for hospitals by allowing expedited throughput of patient thorax exams.

Radiation dose exposure, and the accompanying increased cancer risk, has been the primary downside to the escalating utilization of MDCT imaging in the clinical setting (5). Researchers have since been developing methodologies for the reduction in radiation dose exposure, low-dose MDCT (LDCT), without compromising diagnostic sensitivity. Examples of these LDCT strategies include dose modulation (6) and improved, iterative reconstruction techniques (7). Manufacturers have responded to the increased demand for LDCT in the latest generation CT scanners, improving LDCT scanning performance and incorporating protocols that minimize radiation exposure for dose-sensitive body regions such as the female breasts. Using the newest generation MDCT systems, anthropomorphic pulmonary phantoms with simulated nodules have been studied to examine the relationship between radiation dose (0.1 mGy to 26.4 mGy) and small nodule (1.6 to 12.7 mm) detection (8,9). Findings reveal that while dose does influence the sensitivity of low-density nodule detection, LDCT protocols with doses down to 1 mGy achieve adequate diagnostic performance for the detection of small nodules (8,9).

Lung cancer is an example of a disease for which a large percentage of the high risk population can be easily identified via a smoking history. This, coupled with the high success of other screening programs for prostate, breast and cervical cancers has lead to the investigation of lung cancer screening options. A number of lung cancer screening trials are being conducted in the United States of America and internationally using LDCT imaging (3,10-14). These studies include randomized (13) and non-randomized trials (11,15) some with comparison to alternative modalities, such as CXR (12) or sputum (10). Early findings have shown that LDCT scanning is effective in the detection of early stage lung cancers (12,15-17). However, the published trial data has yet to ascertain if lung cancer screening will significantly reduce mortality and morbidity within the at risk population. Investigations have been launched by The National Lung Screening Trial (NLST) and the Dutch Belgian randomized lung cancer screening trail (NELSON), to evaluate if lung cancer screening by MDCT actually saves lives (3,18). For the NLST, at the time of enrollment closing, nearly 50,000 people with a smoking history were enrolled, making it the largest randomized, controlled lung cancer screening study to date, the results of which are expected at the end of 2010. Preliminary findings from the NELSON trial, which contained 733 participants, have reported negative health-related quality of life affects for patients falling in the indeterminate category following screening. This indeterminate category, reported as having a less than 2.5% risk of cancer, experience lung-cancer-related-distress from the time of initial screening until follow up imaging was completed (~3 months) (3).

CT can be considered the current gold standard for the detection of lung nodules (1,12,17,19,20). However, repeated follow-up CT examinations may be undesirable,

especially for young patients, because of radiation exposure. Although radiation exposure is usually no major issue for cancer patients and LDCT techniques have been proved feasible to reduce the radiation dose, MR imaging does not require any ionizing radiation. MRI might be a valuable tool for the detection of pulmonary nodules in a screening setting, particularly if complex, contrast enhanced imaging protocols could be avoided. Although nodules smaller than 5mm are ignored at CT due to limited specificity in this size, lesions larger than 5mm can be detected using current MR techniques (17-21). In addition, when considering the management guidelines following pulmonary nodule detection with CT, published by the Fleishner Society (21), current pulmonary MR imaging techniques are suggested as having potential for this purpose. Several investigators have addressed this issue by using various sequences with 1.5 Tesla (T) and 3.0 T scanners since 1997. However, patient-related motion artifacts, susceptibility artifacts from the lungs and inferior spatial and temporal resolution as compared with those of CT reduce the quality of MR images of the lungs (22-26). These studies assessed the detection rate for pulmonary nodules which was verified by single-helical CT or MDCT. The detection rates or sensitivities of MR imaging with various sequences on 1.5T and 3.0T systems ranged between 45.5 and 96.0 %, and detection rate or sensitivity of spin-echo sequences were better than those of gradient-echo sequences (22-26).

Recently, Koyama, et al. directly compared capabilities of pulmonary nodule detection and differentiation of malignant from benign nodules between non-contrast-enhanced MDCT and MR imaging using 1.5T system in 161 patients with 200 pulmonary nodules(24). Although overall detection rate of thin-section MDCT was superior to that of respiratory-triggered STIR turbo spin-echo (SE) imaging, there were no significant differences in malignant nodule detection rate between both methods (24). In this study, malignant nodule detection rate including bronchioalveolar carcinoma had no significant difference between thin-section MDCT and non-contrast-enhanced MR imaging, and significantly more benign nodules were missed on non-contrast-enhanced MR imaging. These results are promising for reductions in unnecessary follow-up examinations, intervention and thoracotomy. Therefore, MR imaging on 1.5 T and 3.0 T may have potential for the detection of pulmonary nodules without ionizing radiation exposure. (Fig. 1). In addition, further improvements of MR systems and sequences can be expected to enable pulmonary lung cancer screening as well as whole-body MR screening in the near future.

Pulmonary Nodule Evaluation and Management on CT and MRI

Dynamic CT and Dynamic MR Imaging

Since the asymptomatic pulmonary nodule is one of the most common findings on chest radiographs and CT, it is important to differentiate malignant from benign nodules in the least invasive way and to make as specific and accurate a characterization as possible. Investigators have used CT, MR imaging and FDG-PET or PET/CT to evaluate the radiological features, MR relaxation time, blood supply assessed on dynamic contrast enhancement, water molecule diffusion and metabolism of pulmonary nodules to differentiate malignant from benign nodules with promising results.

Dynamic perfusion CT for the evaluation of lung nodules involves the bolus administration of iodine contrast media and the rapid sequence of CT scan acquisitions to capture the transit of the iodine bolus through the lung nodule. Perfusion CT is a means by which blood flow properties with in a lung nodule may be quantifiably measured in-vivo and presents the opportunity to contribute dynamic features (blood volume, blood flow, permeability, mean transit time, peak enhancement and time to peak enhancement) to those supplied by volumetric CT (Hounsfield Unit, texture, size and shape). Histological markers of tumor angiogenesis have been successfully correlated to diagnosis and prognosis (27-29) for lung

cancer nodules. Hence recent studies have focused on validating perfusion CT outputs against corresponding histological markers and hence to evaluate the diagnostic capabilities of this modality (30,31).

Historically, non-contrast-enhanced MR imaging has shown limited potential for characterizing peripheral lung nodules and masses and identifying the benign nature of nodules due to the low intrinsic signal intensity of the lung parenchyma, the relatively poor spatial resolution and patient-related motion artifacts (32-40). In general, many pulmonary nodules, including lung cancers, pulmonary metastases and low-grade malignancies such as carcinoids and lymphomas are demonstrated as low or intermediate signal intensities on T1-weighted images and as slightly high intensity on T2-weighted images when SE or turbo SE sequences are used (32-40) (Fig. 2). However, it may be possible to characterize several histological types of pulmonary nodules, such as bronchocele, tuberculoma, mucinous bronchioalveolar carcinoma (BAC), hamartoma and aspergilloma on pre- or post-contrast enhanced T1-weighted images and T2-weighted image according to their specific MR findings (41-47).

Recently, diffusion-weighted imaging (DWI) has been suggested as new method for nodule detection and / or evaluation including subtype classification of pulmonary adenocarcinoma (48-50). This technique is suggested as can assess water molecule diffusion within tissue by using apparent diffusion coefficient (ADC) measurements or signal intensity ratio between the lesion and spinal cord ratio. Although no direct comparisons between DWI and PET or PET/CT were present, these studies may demonstrate the real significance of DWI for non-contrast-enhanced MR assessment of pulmonary nodule in near future.

Although enhancement levels vary due to underlying microscopically determined pathologic conditions such as tumor angiogenesis, tumor interstitial spaces, the presence or absence of fibrosis, and scarring and necrosis within the tumor, malignant pulmonary nodules show homogeneous enhancement but at a variety of levels on T1-weighted images after administration of contrast media (32-40,51,52). Consequently, when using pre- and post-contrast enhanced conventional T1-weighted images and T2-weighted images, clinicians in routine clinical practice often face a diagnostic dilemma in distinguishing malignant from benign pulmonary nodules such as organizing pneumonia, benign tumors and inflammatory nodules (32-40) (Fig. 3). It has therefore been suggested that enhancement patterns or blood supply evaluated with dynamic contrast-enhanced MR imaging may be helpful for diagnosis and management of pulmonary nodules (32-40).

As a result of advances in MR systems and pulse sequences, there are now three major methods for dynamic MR imaging of the lung. Many investigators have proposed dynamic MR imaging be used for two-dimensional (2D) SE or turbo SE sequences or for various types of 2D or three-dimensional (3D) gradient-echo (GRE) sequences and that enhancement patterns within nodules and/or parameters determined from signal intensity-time course curves be assessed visually. These curves represent first transit and/or recirculation and washout of contrast media under breath holding or repeated breath holding during 5 minutes (32-40). Although there are various dynamic MR techniques for distinguishing malignant nodules from benign nodules at small or large populations, reported sensitivities range from 94 to 100%, specificities from 70 to 96%, and accuracies of more than 94% (32-40). These specificities and accuracies for dynamic MR imaging are superior to those reported for dynamic CT, and almost equal to or superior to those for FDG-PET or PET/CT (40). In addition, dynamic MR imaging with 3D GRE sequence require the less than 30 sec breath holding for all data acquisition, although FDG-PET or PET/CT need almost 2 hour after injection of FDG. Therefore, dynamic MR imaging may perform a

complementary role in the characterization of pulmonary nodules assessed with FDG-PET or PET/CT.

Considering the management of pulmonary nodules in clinical practice, it may be helpful to differentiate pulmonary nodules requiring further intervention and treatment (low- or high grade malignant tumors and active infectious nodules) from pulmonary nodules requiring no further evaluation (benign tumors and chronic infectious nodules) rather than to differentiate between malignant nodules and other nodules. For this latter differentiation, ultra-fast dynamic MR imaging can divide all nodules into the two categories (Figs. 3 and 4) (34,40) This means that it may be better to use dynamic MR imaging in a complementary role to CT and FDG-PET or PET/CT to determine whether further intervention and treatment are indicated rather than to differentiate pulmonary nodules into malignant nodules and other nodules in routine clinical practice (40). The value of this approach may be of limited value in geographic regions where endemic fungal infections such as histoplasmosis or coccidiosis occur.

Dual Energy CT for Lung Nodule Evaluation

Dual energy (DE) x-ray investigations began with digital CXR to allow advanced tissue selectivity; eliminating the ribs in tissue selective images to augment nodule detection and enhancing calcifications in bone selective images to distinguish calcified nodules (53). From DE CXR the value in nodule detection and characterization has been confirmed and the technology progressed to DE CT (54-56). Original experiments in DE CT focused less on the impact on dose and more on the resulting image quality. However, with advanced CT system technology the compromise is no longer required and the superior imaging capabilities of DE CT can be achieved with minimal increases on radiation dose. One drawback of DE CT is the increased cost of the hardware and maintenance fees due to the inclusion of two x-ray tubes within the system.

Chae et al. examined the clinical utility of DE CT along with the dose implications using 49 patients (54). Comparisons were drawn between non-enhanced weighted average, virtual non-enhanced, enhanced weighted average and iodine-enhanced images. The practical use of these datasets are the ability to using a single scanning approach to generate both data useful for evaluating calcification (virtual non-enhanced) and distinguishing benign from malignant nodules (iodine-enhanced), there by maintaining diagnostic power for a reduced radiation dose scanning procedure. Comparable diagnostic accuracy – 82% to 71% - was found using the iodine-enhanced data versus the degree of enhancement. While the size of detected nodules was smaller on the virtual non-enhanced data than on the true non-enhanced weighted average data, the detection rate was 85%. Also, the radiation dose between the DE CT and single-energy CT protocol was not significantly different ($p = 0.67$).

Visualization of Volumetric Medical Image Data

The escalating use of volumetric imaging modalities such as MR and CT within the clinical environment, in conjunction with the increasing resolution of the resulting datasets has lead to an exponential growth of data to be viewed and interpreted by radiologists. Challenges are faced in the optimal method to visualize the 3D datasets, extracting out the valuable information and balancing time efficient case management.

The most common approach for the visualization of volumetric medical image data is the three window, cross-sectional view; with axial, sagittal and coronal view plane. The advantage of this visualization method is the controlled progression through the data, advancing through 2D axial image slices from the trachea to the diaphragm in thorax studies to systematically scan the data for nodules. Until recently, the volumetric visualization of

medical image datasets with rendered views required high performance computing power and customized software development. Today, average desktop computer systems, with relatively affordable upgraded graphics cards, are capable of manipulating 3D medial image datasets and software packages are available to assist with visualization, segmentation and rendering tasks of volumetric medical image data.

Volumetric projections and/or reconstructions can facilitate comprehension of spatial relationships between structures and have been shown to improve the diagnosis of small nodules (Fig 5). Eibel et al. compared the detection of small pulmonary nodules in CT using maximum intensity projections (MIP) and the standard axial reconstructions. While the detection of pulmonary nodules greater than 5mm was equal between the two visualization methods, there was a statistically significant ($p<0.05$) improvement in detection of nodules less than 5 mm using the MIP view (57). Differences, although not statistically significant, were also observed by Wang et al. when studying the ergonomic efficiency between standard axial view, MIP and stereoscopic (58). However, highlighted by this study was the prevailing difficulty in comparing interpretation methods and compensating for the inherent preference for routine, as is the standard axial view, versus the learning curve required with alternative approaches. In many cases the practices and diagnostic measures have not developed at the same rate as the technology being improved.

MR, for which the datasets can be large and complex, can greatly benefit from effective visualization techniques. Recently, information visualization has been combined with data mining to develop a novel analysis and visualization method for DCE-MR tumor datasets (59). While this technique has not yet been applied to lung nodules, evidence of correspondence between the boundaries identified by the approach and histologically identified tissues was presented.

Computer Aided Detection and Diagnosis

Computer aided detection/diagnosis (CAD) algorithms incorporate image analysis and pattern recognition techniques in order to identify and describe areas of interest in an image dataset. In many cases, the area of interest is a specific pathology such as a lung nodule in a digital image dataset, such as CXR, CT, CT/PET or MR. The relatively recent application of MR for lung nodule detection and management means the CAD development for this modality has not yet been reported in the literature. However, a great potential exists in the use of CAD for exploring the many features captured by different MR sequences. The development of CAD for MR should be greatly assisted by the techniques already established for CT.

CAD systems are becoming increasingly important in the clinical setting, serving as a second reader in image interpretation, effectively improving the detection accuracy and consistency of pulmonary nodules in CXR (60) and CT (61,62). Awai et al. compared the nodule detecting performance of five radiologists and five radiology residents in fifty chest CT scans. Statistically significant improvements in lung nodule detection were achieved for all radiologists using the CAD system ($p < 0.1$), with a true positive rate of 94% (61).

The challenge that is found with the early identification of small pulmonary nodules through CT imaging is distinguishing those which require treatment, the so called ‘actionable nodule’, from the benign lesions which do not require treatment. In some cases CAD will extend beyond the detection of pathology, to also incorporate a diagnosis element which aims to provide a likelihood of malignancy for detected nodules. Methods which utilize features from unenhanced CT (63), perfusion CT (64,65) and PET/CT have been developed (66).

CAD system development for the volumetric segmentation of suspicious lung nodules is also highly important for the long term evaluation of suspicious lung nodules or for the evaluation of response to treatment of malignant nodules. There is a significant decrease is precision accompanied by intra-observer/inter-observer variability induced through the manual segmentation of lung nodules (67) which may be improved through CAD size estimation techniques (68,69) and volumetry (70,71). This area of CAD development would also be of immense benefit to MR in which the same challenges exist in determining and monitoring nodule dimensions.

A current limitation in the comparison of CAD systems for lung nodule detection and classification is the variation in training and testing datasets, making the cross comparison of methods extremely challenging. Variability in the imaging system hardware, imaging protocol and reconstruction protocol along with the diversity of the pulmonary nodule case set contributes significantly to CAD performance. Some studies have been conducted using phantom lung nodule datasets to investigate the influence of these image acquisition variabilities in both CT and MR (72,73). In order to enhance the development of CAD systems and their effective, unbiased, comparison the National Cancer Institute established the Lung Image Database Consortium (LIDC) (74). The LIDC has developed an extensive database of chest CT scans to be accessible to researchers for education, training and the development and testing of CAD approaches. A similar database for chest MR scans is required to facilitate the creation of effective MR based CAD approaches.

CT Assisted Biopsy for Diagnosis

Histology remains the ground truth for diagnosis of suspicious lung nodules and hence, where possible, biopsy of the nodule is used to aid in the treatment planning process. CT provides an accurate, 3D anatomical depiction of the lung, distinguishing not only the nodule but also the surrounding structures such as airways, blood vessels and parenchyma. Having a method of investigating the location and surrounding tissues of a nodule prior to any intervention can be a great advantage in planning the biopsy approach. Recent advances have extended upon this, to create user friendly systems to directly guide biopsy procedures.

Virtual bronchoscopy is achieved through the identification of the airways with in the volumetric CT data and the computer graphic rendering of these structures to mimic the standard bronchoscopy view (Fig 6). As the CT data also contains additional information, including identified suspicious pulmonary nodules, these areas can be highlighted using the virtual bronchoscopy view and used to guide bronchoscopic biopsy. Displayed along with the virtual bronchoscopy view, are directional indicators to highlighted pulmonary nodules to aid the bronchoscopists navigation to areas for biopsy (75). Initial approaches for the use of virtual bronchoscopy, utilized a fixed movie generated from the CT data to train bronchoscopists in navigation and targeting regions of interest (76), however, increased computing power has allowed for real time virtual bronchoscopy in which the CT based virtual bronchoscopy view is matched and continually updated to the current bronchoscopy view, allowing superior navigation in the clinical environment (75,77).

Merritt et al. compared the performance of twelve bronchoscopists in localizing 10 artificial lesions within a lung phantom using standard bronchoscopy procedure or bronchoscopy accompanied by virtual bronchoscopy image guidance (77). Nodule localization, as defined by a biopsy position error ≤ 5 mm, increased more than two fold from 43% using standard procedure to 94% with the image guided approach (77). McLennan et al. investigated the ability of virtual bronchoscopy image guidance in improving lymph node sampling, an important aspect of lung cancer staging, and found an improvement from 66% using standard procedure to 92% with imaging guidance (78). Building upon the success of virtual bronchoscopy guidance, integrated bronchoscopy techniques have been explored in the

literature, merging structure from CT with other assistive diagnostic tools such as bronchoscopic color analysis and fluorescence or PET to aid the accurate localization of biopsy targets (79,80). Based on the ability of ultra-fast dynamic MR to characterize lung nodules into those requiring intervention (malignant and active infection) versus those not requiring intervention (benign) the future incorporation of this modality into integrated virtual bronchoscopy techniques may be beneficial (34,40).

Electromagnetic navigation bronchoscopy (ENB) is a novel technology which builds upon the virtual bronchoscopy image guidance systems. Developed to assist the navigation to peripheral pulmonary nodules which are inaccessible with a standard bronchoscopic approach. A magnetic navigation board creates a magnetic field around the patient's thorax and a sensor probe is used to track the progression of biopsy tools through the lung and display the real-time location on the previously acquired volumetric CT images (81-84). One of the largest advantages of the ENB is the correlation between the exact coordinates of the nodule identified in the CT data and the corresponding location in the patient, accompanied by the 360 degree steerable distal tip of the probe. Studies using ENB have progressed from animal models (82) to human patients (83,84), to evaluate the safety and accuracy of the technique. Conclusive diagnostic yield of between 69% and 77% have been reported and have been coupled with 0 to 8% adverse outcomes (pneumothorax) (83,84). While these results are promising, the diagnostic accuracy and adverse outcomes are challenging to compare directly to the alternative biopsy method - CT-guided transthoracic needle biopsy which reports accuracy of 83% although with 5.5% adverse outcomes (85) – due to differences in inclusion criteria.

Linking Ground Truth Pathology to Radiological Imaging

Histological classifications of lung cancer have been established by the World Health Organization (WHO) for treatment planning and prognostic purposes. However, in-vivo imaging is playing an increasing role in the identification and preliminary characterization of lung nodules. The correlation between in-vivo imaging representations of lung nodules and the corresponding ‘ground truth’ histopathology is required to maximize the diagnostic potential of imaging modalities such as CT and MR.

For many years, it has been acceptable to correlate histological findings with non-destructive imaging observations by general comparison (31,86,87). However, due to the estimated correspondence between the datasets, there is a heavy reliance on qualitative interpretation by the human observer to link the information content. While approximated correlations can provide valuable, qualitative insight to in-vivo representations, precise correlations are required to generate more useful, quantitative results.

Recently, a process model was established which permits direct voxel-to-voxel association between CT imaging and volumetric histopathological data in human lung cancer (88-90). This process was established to relate the complex 3D histopathology of pulmonary nodules to corresponding CT data and will allow future quantitative evaluation. Human patients with identified lung nodules requiring surgical resection via lobectomy, were enrolled in the study. Imaging was performed before the nodule was removed from the patient and on the lobectomy specimen after surgery. The process model involved sequential imaging stages which had increasing resolution, progressing from in-vivo CT to ex-vivo CT to 3D microscopic evaluation. Incorporated was a specifically designed microscopy system, the large image microscope array (LIMA), designed to serve as a reliable structural reference between the radiological datasets and the histopathological sections (91). Through the establishment of a structural reference (LIMA), rigid and non-rigid registration techniques were employed to accurately align the CT data and the histopathological data to a common

coordinate system (Fig. 7). Future expansion of this process model to include perfusion CT, PET/CT and MR datasets to the underlying 3D histopathology content of pulmonary nodules would be highly valuable.

Lung Cancer Staging

The international TNM classification proposed by the International Union against Cancer (UICC) has been widely used in the investigation and treatment of lung cancer. Accurate staging is essential for determining the appropriate treatment option for lung cancer patients. Staging will indicate if treatment may be achieved through surgical resection and whom may benefit from chemotherapy, radiotherapy, or both(92). Currently, CT, FDG-PET or PET/CT, are considered useful for more precise assessment of tumor extent because of their multiplanar capability and for accurate diagnosis of metastastic lymph nodes by analyzing the glucose metabolism of cancer cells in lung cancer patients. However, since 1991 it has been suggested that MR imaging may also be useful for mediastinal and chest wall invasions due to its multiplanar capability and superior to CT contrast resolution of tumor and mediastinum and/or tumor and chest wall (93). Recent advances in MR systems, improved or newly developed pulse sequences and/or utilization of contrast media has resulted in improved TNM staging for lung cancer patients.

Assessment of T Classification

Many surgeons consider minimal invasion of mediastinal fat as resectable (94), so that clinicians want to know whether minimal mediastinal invasion (T3 disease) or actual invasion (T4 disease) has occurred before considering surgical resection. The accuracy of computed tomography (CT) for evaluating hilar and mediastinal invasion of lung cancer has been investigated extensively over the last two decades. Sensitivity for assessment of mediastinal invasion by single-detector or electron beam CT with or without the use of helical scanning ranged from 40% to 84% and specificity from 57% to 94% (94-98).

Currently, PET or PET/CT is routinely adapted for lung cancer staging. FDG-PET imaging is of potential use in assessing the metabolic activity of the primary lung cancer, which reflects cell turnover rate and may indicate the biologic aggressiveness of the cancer. However, no major papers discussed the capability for assessment of T-factor assessment on PET or PET/CT. Only a paper recently published by Yi et al addressed this issue with comparison with whole-body 3.0 T MR imaging(99). In this study, the primary tumor was correctly staged in 101 (82%) patients at PET/CT and in 106 (86%) patients at whole body 3.0 T MR imaging, and the difference in accuracies between integrated PET/CT and whole-body MR imaging was not statistically significant. Due to the limited accuracy of the functional data from PET with the morphological information as derived from CT or MR, PET is not useful in T-Staging.

Mediastinal Invasion Assessment—The RDOG study compared CT with MR imaging for 170 patients with non-small cell lung cancer, although only T1-weighted images obtained without the use of cardiac or respiratory gating techniques were assessed in this study (93). Although there was no significant difference between the sensitivity (63% and 56% for CT and MR imaging, respectively) and the specificity (84% and 80%) for distinguishing between T3-T4 tumors and T1-T2 tumors in this study, the RDOG reported that 11 patients showed mediastinal invasion and that the superior contrast resolution of MR imaging conferred a slight but statistically significant advantage over CT for accurate diagnosis of mediastinal invasion. In addition, delineation of tumor invasion of pericardium (T3) or heart (T4) was superior on MR imaging to that on CT scan when the cardiac-gated T1-weighted sequence was used for improved avoidance of cardiac motion artifacts (100). The normal pericardium has low signal intensity. Direct invasion of the cardiac chambers is

readily demonstrated on T1-weighted images, because blood flowing through the cardiac chambers is signal void, so that the tumor is conspicuous because of its higher signal intensity. However, the accuracy of minimal mediastinal invasion assessment by both CT scanning and MR imaging is limited because it depends on visualization of the tumor within the mediastinal fat (101).

Recent advances in MR systems, improved pulse sequences and utilization of contrast media have resulted in the introduction of new MR imaging techniques for assessment of mediastinal invasion of lung cancer. Contrast-enhanced MR angiography has been used for assessment of cardiovascular or mediastinal invasion (102,103). Ohno et al described a series of 50 NSCLC patients with suspected mediastinal and hilar invasion of lung cancer visualized with contrast-enhanced CT scans, cardiac-gated MR imaging, and non-cardiac- and cardiac-gated contrast-enhanced MR angiographies (103). In this study, sensitivity, specificity and accuracy of contrast-enhanced MR angiography for detection of mediastinal and hilar invasion ranged from 78 to 90%, 73 to 87%, and 75 to 88%, respectively. These values were higher than those of contrast-enhanced single helical CT and conventional T1-weighted imaging (103). Thus, contrast-enhanced MR angiography is thought to improve the diagnostic capability of MR imaging for mediastinal and hilar invasion.

Since clinical installation of MDCT, thin-section multiplanar reformatted (MPR) imaging from thin-section volumetric MDCT data has been utilized for evaluation of T classification in routine clinical practice. Higashino et al. suggested that mediastinal invasion that can be assessed from thin-section coronal MPR images with 1 mm section thickness with greater sensitivity (86 %), specificity (96 %) and accuracy (95 %) than can be achieved with routine MDCT with 5 mm section thickness (sensitivity: 71 %, specificity: 93 %, accuracy: 90 %), and with slightly better specificity (93 %) and accuracy (92 %) than with thin-section axial MDCT with 1 mm section thickness, although statistical significance were not present (104). Although MR imaging is considered to show superior tissue contrast to that of MDCT, with similar multiplanar capability, faster scan time and better spatial resolution of thin-section MPR imaging may result in better assessment of mediastinal invasion in NSCLC patients than previously described MR techniques. Further investigations as well as comparative studies of thin-section MPR imaging and previously described or newly developed MR imaging techniques thus seem to be warranted to determine the actual significance of MR imaging for assessment of mediastinal invasion in routine clinical practice.

Chest Wall Invasion Assessment—As well as mediastinal invasion, chest wall invasion used to be considered a contraindication for surgical excision of lung cancer, but recent surgical advances have made chest wall excision feasible for the treatment of locally aggressive lung cancer and provide patients a better chance of survival (105). Preoperative visualization of chest wall invasion may therefore be helpful for surgical planning. On conventional CT, rib destruction is the only reliable sign of chest wall invasion since soft tissue masses in the chest wall correlate statistically with chest wall invasion. However, they are not reliable indicators for an individual patient, so that focal chest pain may still be the most reliable indicator of chest wall invasion. In fact, the reliability of conventional CT assessment of chest wall invasion in lung cancer patients varies widely with reported sensitivities ranging from 38-87% and specificities from 40-90% (94). In addition to the technique of inducing artificial pneumothorax described elsewhere (106), Murata et al reported that dynamic expiratory multi-section CT reviewed as a cine loop was 100% accurate for identification of both chest wall and mediastinal invasion (107).

Because of its multiplanar capability and better tissue contrast resolution compared to CT, MR imaging has also been advocated as effective for assessment of chest wall invasion (93,108-111). Sagittal and coronal MPR images are better than axial CT images for

displaying the anatomical relationship between tumor and chest wall structures (93,108-112). MR imaging shows infiltration or disruption of the normal extra pleural fat plane on T1-weighted images or parietal pleural signal hyper intensity on T2-weighted images (93,108-112). In addition, when STIR turbo SE imaging is used for this purpose, it can demonstrate lung cancer as high signal intensity within the suppressed signal intensities of chest wall structures, enabling clinicians to determine the tumor extent within chest wall. Moreover, Padovani et al have suggested that the diagnostic yield can be further improved by intravenous administration of contrast media (110). In addition, superior sulcus or Pancoast tumors have proven to be good indication for MR imaging. Since superior sulcus tumors occur in close proximity to the lung apex, their imaging should include an evaluation of the relationship between the tumor and the brachial plexus, subclavian artery and vein, and adjacent chest wall. The axial scan plane of a CT scan is suboptimal for examining the lung apex where superior sulcus tumors are located, while direct sagittal and coronal MR images have been shown to be superior to CT for evaluating the local extent of disease in patients with superior sulcus tumors (93,110,111).

Sakai et al used dynamic cine MR imaging rather than static MR imaging during breathing for evaluating chest wall invasion in lung cancer patients (113). This study evaluated the movement of the tumor along the partial pleura during the respiratory cycle displayed with a cine loop in a manner similar to dynamic expiratory multi-section CT (107). Where the tumor had invaded the chest wall, it was fixed to the chest wall, and without invasion, the tumor was seen to move freely along the partial pleura. In this study, the sensitivity, specificity, and accuracy of dynamic cine MR imaging for the detection of chest wall invasion were 100, 70, and 76%, respectively, and those of conventional CT and MR imaging were 80, 65, and 68% (113). Of special significance is that the negative predictive value in this study was 100% without any need for ionizing radiation exposure. Dynamic cine MR imaging, when used in conjunction with static MR imaging, should therefore also be considered useful for further improvement of the assessment of chest wall invasion in lung cancer patients.

Currently, multiplanar capability, faster scan time and better spatial resolution of thin-section MPR images may improve the diagnostic capability of CT for evaluation of chest wall invasion in NSCLC patients similar to that of mediastinal invasion, although MR imaging is considered to have superior tissue contrast compared with MDCT (104). Thin-section sagittal MPR imaging with 1 mm section thickness could significantly improve diagnostic accuracy for chest wall invasion in comparison with routine MDCT with 5 mm section thickness, and showed slightly better diagnostic capability than thin-section MDCT with 1 mm section thickness (104). Therefore, further investigations as well as comparative studies of thin-section MPR imaging and MR imaging used as described here, or of newly developed techniques will be needed to determine the actual significance of MR imaging for assessment of chest wall invasion in routine clinical practice.

Distinguishing Lung Cancer from Secondary Change—Distinguishing primary lung cancer from secondary change is important for assessment of tumor extent and the therapeutic effect of chemotherapy and/or radiotherapy. While the therapeutic effect of conservative therapy has been assessed by using World Health Organization (WHO) criteria or response evaluation criteria in solid tumors (RECIST) criteria (114,115), it would be difficult to use CXR or plain or contrast-enhanced CT to evaluate tumor extent or therapeutic effect for cases with atelectasis or obstructive pneumonia.

MR imaging, on the other hand, has potential for distinguishing lung cancer from secondary change due to atelectasis or pneumonitis (52). In some cases, it can be difficult to distinguish lung cancer from post-obstructive atelectasis or pneumonitis because these secondary

changes tend to be enhanced to a similar degree as the central tumor on contrast-enhanced CT scan. On T2-weighted MR imaging, however, post-obstructive atelectasis and pneumonitis often show higher signal intensity than does the central tumor (93). Bourgounin et al evaluated the histologic findings of obstructive pneumonitis or atelectasis in patients who had undergone surgical resection of lung cancer and who had been evaluated preoperatively with MR imaging (116). They found that cholesterol pneumonitis and mucus plugs displayed higher signal intensity than the tumor on T2-weighted images, while atelectasis and organizing pneumonitis were isointense to the tumor. Kono et al described a series of 27 patients with central lung cancer associated with atelectasis or obstructive pneumonitis (39). These patients were examined with post-contrast enhanced T1-weighted MR imaging and the central tumor could be differentiated from adjacent lung parenchymal disease in 23 out of 27 patients (85%). The tumor was of lower signal intensity than the adjacent lung disease in 18 cases (67%) and of higher signal intensity in five (18%). These differences in signal intensity between primary tumor and secondary change were considered to be due to the presence of invasion of pulmonary vasculatures. Therefore, the use of T2-weighted or post-contrast enhanced T1-weighted images for assessment of tumor size and secondary change may be helpful for precise evaluation of tumor extent at the initial staging and for accurate prognosis for patients and assessment of therapeutic effect after conservative therapy and/or for comparative studies of standard and new chemo- and/or radiotherapy regimens (117).

Assessment of N Classification

CT has been the standard noninvasive modality for staging of lung cancer. Enlarged lymph nodes (i.e. with a short axis of more than 10 mm or a long axis of more than 15 mm) are considered to be metastastic. Although an increase in the size of mediastinal lymph nodes correlates with malignant involvement in patients with lung cancer, the sensitivity and specificity of this finding are not very high because lymph nodes can be enlarged due to infection or inflammation. In addition, small nodes can sometimes contain metastatic deposits. The RDOG reported that the sensitivity and specificity of CT for *N* classification were only 52% and 69%, respectively (93), while the Leuven Lung Cancer Group (LLCG) corresponding values of 69% and 71% (118). Due to the substantial limitation of CT for depicting mediastinal lymph node metastases, additional mediastinoscopy with biopsy is necessary for adequate assessment of hilar and mediastinal nodes (93,119,120).

Since the 1990s, FDG-PET has been used for differentiation between metastatic and non-metastatic lymph nodes based on the biochemical mechanism of increased glucose metabolism or tumor cell duplication (121-125). However, elevated glucose metabolism may occur secondary to tumor, infection or inflammation, and spatial resolution in PET is inferior to that of CT and MR, so that the diagnostic capability of the FDG-PET imaging is limited (124).

Since the introduction of MR imaging for assessment of lung cancer, MR imaging criteria for tumor involvement within lymph nodes depend on lymph node size, similar to CT criteria. In some cases, however, histologic examination has proved that a normal-sized regional lymph node may have metastases, and that nodal enlargement can be due to reactive hyperplasia or other nonmalignant conditions. Detection by MR of calcium, indicative of benignancy, is also limited compared with that by CT. The direct multiplanar capability of MR imaging, however, is an advantage for the detection of lymph nodes in areas that are sub-optimally imaged in the axial plane, such as in the aorto-pulmonary (AP) window and subcarinal regions (93,125).

Recently, cardiac- and/or respiratory-triggered conventional or black-blood STIR turbo SE imaging has been recommended for detection of metastatic tumors and metastatic lymph

nodes (126-128). This novel sequence may make it possible for the signal intensity of lymph nodes to be quantitatively assessed by means of comparison with a 0.9% normal saline phantom (126-128). The STIR turbo spin-echo (SE) is a simple sequence, which can be easily incorporated into clinical protocols to yield net of T1- and T2-relaxation times. On STIR turbo SE images, metastatic lymph nodes are indicated as high signal intensity and non-metastatic lymph nodes as low signal intensity (Fig. 8 and 9). Several studies have reported that sensitivity, specificity and accuracy of quantitatively and qualitatively assessed STIR turbo SE imaging ranged between 83.7 % and 100.0 %, between 86.0 % and 93.1 %, or between 86.0 % and 92.2 % on a per-patient basis (126-128). Direct and prospective comparisons with CT on a per-patient basis demonstrated that sensitivity and accuracy of quantitatively and qualitatively assessed STIR turbo SE imaging are significantly higher (127). In addition, direct and prospective comparisons with co-registered FDG-PET/CT showed that quantitative sensitivity and accuracy of STIR turbo SE imaging were significantly higher (128). STIR turbo SE imaging thus should be considered as capable of enhancing the diagnostic capability of *N* classification due to not only its multiplanar capability but also its sensitive and accurate assessment of relaxation time differences between metastatic and non-metastatic lymph nodes, and should therefore be considered at least as valuable as FDG-PET/CT.

In the last decade, other MR techniques such as contrast-enhanced MR imaging with super-paramagnetic or ultra-small super-paramagnetic contrast agents (129-131), combined radiologic and metabolic information derived from T2-weighted image and PET (132), and DWI (133) have also been suggested as useful similar to STIR turbo SE imaging. However, these techniques have not been directly compared with FDG-PET or FDG-PET/CT, and sample sizes in these studies were small. Therefore, further studies may be warranted to demonstrate clinical significance of the above-mentioned technique in this setting.

Assessment of M Classification

Patients with distant metastases carry a very poor prognosis and are generally treated with chemotherapy, radiotherapy, or both or with optimal supportive care. The observation of metastasis in patients with NSCLC has major implications for management and prognosis. Extra-thoracic metastases are present in approximately 40 % of patients with newly diagnosed lung cancer at presentation, most commonly in the adrenal glands, bones, liver, or brain (134,135). The accurate diagnosis of extra-thoracic metastases may be help clinicians to provide the most appropriate treatment and/or management for lung cancer patients. Therefore, for purpose of TNM classification, the current recommendation from the American College of Chest Physicians (ACCP) indicates that further diagnostic testing is necessary to confirm the presence of disease in patients with abnormal findings on clinical evaluation (136).

FDG-PET is not suitable for the detection of brain metastases since the sensitivity of PET is low due to the high glucose uptake of normal surrounding brain tissue. Therefore, CT and/or MR imaging remains the method of choice for screening brain metastases. However, findings of a recent randomized trial suggest that the addition of whole-body FDG-PET scanning to a conventional workup can identify more patients with extra-thoracic metastases among those with suspected NSCLC (137).

Recent advances in MR techniques such as fast imaging and moving table techniques make it possible to perform total body MR imaging, and considered as a single, cost-effective imaging test for patients with metastatic carcinoma in patients with various malignancies or an unknown primary (138-146).

When comparing whole-body MR imaging with FDG-PET for the M-classification capability of head and neck metastases, including brain metastases, the accuracy (80.0 %) of whole-body MR imaging was significantly better than that of FDG-PET (73.3 %). Excluding brain metastases from head and neck metastases, resulted in no significant differences in sensitivity, specificity and accuracy between whole-body MR imaging and FDG-PET (145).

Recently, whole-body DWI is suggested as useful for oncology imaging. When this technique adapted for M-stage assessment including brain metastasis in non-small lung cancer, diagnostic accuracy of whole-body MR imaging with DW imaging (87.7 %) had no significant difference with that of integrated FDG-PET/CT (88.2 %) on a per-patient basis (146). In addition, accuracy of integrated FDG-PET/CT (90.4 %) was significantly higher than that of whole-body MR imaging without DW imaging (85.8 %, $p<0.05$), when excluded brain metastasis (146). Therefore, whole-body MR imaging with DW imaging can be used for M-stage assessment in patients with NSCLC with accuracy as good as that of integrated PET/CT; in addition, when whole-body DW imaging is adopted as an adjunct for whole-body MR imaging without whole-body DW imaging, the diagnostic accuracy of whole-body MR examination can be improved.

Conclusion

We have reviewed the current developments in the application of CT and MR for the detection and management of pulmonary nodules and lung cancer staging. Due to its superior resolution and scan time, CT has been accepted as the modality of choice for pulmonary nodule investigations and the maturity of approaches and tools for CT based analysis of pulmonary nodules places the modality as the clinical choice. Exciting technological developments have been achieved using CT imaging, including virtual bronchoscopy and biopsy guidance systems as well as CAD approaches for nodule identification and characterization. The creation of an open access database of chest CT datasets, featuring pulmonary nodules, by the LIDC will assist the development and comparison of CAD techniques, further accelerating the progress of this technology.

Low-dose imaging protocols are being widely employed for the CT imaging of pulmonary nodules, however, the increasing clinical applications of CT and the possibility of CT screening in the future, continue to make medical radiation exposure a concern. The many developments for the application of MR for the detection and evaluation of lung nodules staging have been reviewed. Comparisons between the accuracies and sensitivities of CT and MR have been drawn for the detection, staging and management of primary pulmonary nodules. Of particular interest is the emerging application of dynamic MR imaging for the distinction between nodules requiring follow up treatment (malignant or active infectious nodule) and those requiring no intervention (benign or chronic infectious nodule).

While the potential of MR has been indicated, further development of protocols, clinical trials and advanced analysis tools are required to define a place for MR in the clinical setting. An advantage for the progression of MR applications is the ability to build upon what has already been established for CT, such as existing CAD approaches. With new developments in the direct association between in-vivo imaging and underlying 3D histopathology of pulmonary nodules, quantitative exploration of the tissue specific distinguishing powers of CT and MR is possible.

Acknowledgments

Sources of Support: McLennan: NIH R01 CA129022-01

References

1. Hansell DM, Bankier AA, MacMahon H, McLoud TC, Muller NL, Remy J. Fleischner Society: glossary of terms for thoracic imaging. Radiology. 2008; 246(3):697–722. [PubMed: 18195376]
2. van Klaveren RJ, Oudkerk M, Prokop M, et al. Management of lung nodules detected by volume CT scanning. N Engl J Med. 2009; 361(23):2221–2229. [PubMed: 19955524]
3. van den Bergh KA, Essink-Bot ML, Borsboom GJ, et al. Short-term health-related quality of life consequences in a lung cancer CT screening trial (NELSON). Br J Cancer. 2010; 102(1):27–34. [PubMed: 19935789]
4. Yang GZ, Firmin DN. The birth of the first CT scanner. IEEE Eng Med Biol Mag. 2000; 19(1):120–125. [PubMed: 10659438]
5. Brenner DJ, Hall EJ. Computed tomography--an increasing source of radiation exposure. N Engl J Med. 2007; 357(22):2277–2284. [PubMed: 18046031]
6. Matsubara K, Takata T, Koshida K, et al. Chest CT performed with 3D and z-axis automatic tube current modulation technique: breast and effective doses. Acad Radiol. 2009; 16(4):450–455. [PubMed: 19268857]
7. Thibault JB, Sauer KD, Bouman CA, Hsieh J. A three-dimensional statistical approach to improved image quality for multislice helical CT. Med Phys. 2007; 34(11):4526–4544. [PubMed: 18072519]
8. Silverman JD, Paul NS, Siewerdsen JH. Investigation of lung nodule detectability in low-dose 320-slice computed tomography. Med Phys. 2009; 36(5):1700–1710. [PubMed: 19544787]
9. Paul NS, Siewerdsen JH, Patsios D, Chung TB. Investigating the low-dose limits of multidetector CT in lung nodule surveillance. Med Phys. 2007; 34(9):3587–3595. [PubMed: 17926962]
10. Swensen SJ, Jett JR, Hartman TE, et al. Lung cancer screening with CT: Mayo Clinic experience. Radiology. 2003; 226(3):756–761. [PubMed: 12601181]
11. Sone S, Nakayama T, Honda T, et al. CT findings of early-stage small cell lung cancer in a low-dose CT screening programme. Lung Cancer. 2007; 56(2):207–215. [PubMed: 17258349]
12. Henschke CI, McCauley DI, Yankelevitz DF, et al. Early lung cancer action project: a summary of the findings on baseline screening. Oncologist. 2001; 6(2):147–152. [PubMed: 11306726]
13. Gohagan J, Marcus P, Fagerstrom R, Pinsky P, Kramer B, Prorok P. Baseline findings of a randomized feasibility trial of lung cancer screening with spiral CT scan vs chest radiograph: the Lung Screening Study of the National Cancer Institute. Chest. 2004; 126(1):114–121. [PubMed: 15249451]
14. Xu DM, van der Zaag-Loonen HJ, Oudkerk M, et al. Smooth or attached solid indeterminate nodules detected at baseline CT screening in the NELSON study: cancer risk during 1 year of follow-up. Radiology. 2009; 250(1):264–272. [PubMed: 18984780]
15. Nawa T, Nakagawa T, Kusano S, Kawasaki Y, Sugawara Y, Nakata H. Lung cancer screening using low-dose spiral CT: results of baseline and 1-year follow-up studies. Chest. 2002; 122(1): 15–20. [PubMed: 12114333]
16. Gohagan JK, Marcus PM, Fagerstrom RM, et al. Final results of the Lung Screening Study, a randomized feasibility study of spiral CT versus chest X-ray screening for lung cancer. Lung Cancer. 2005; 47(1):9–15. [PubMed: 15603850]
17. Swensen SJ, Jett JR, Hartman TE, et al. CT screening for lung cancer: five-year prospective experience. Radiology. 2005; 235(1):259–265. [PubMed: 15695622]
18. Church TR. Chest radiography as the comparison for spiral CT in the National Lung Screening Trial. Acad Radiol. 2003; 10(6):713–715. [PubMed: 12809426]
19. Libby DM, Smith JP, Altorki NK, Pasmantier MW, Yankelevitz D, Henschke CI. Managing the small pulmonary nodule discovered by CT. Chest. 2004; 125(4):1522–1529. [PubMed: 15078769]
20. Bach PB, Silvestri GA, Hanger M, Jett JR. Screening for lung cancer: ACCP evidence-based clinical practice guidelines (2nd edition). Chest. 2007; 132(3 Suppl):69S–77S. [PubMed: 17873161]
21. MacMahon H, Austin JH, Gamsu G, et al. Guidelines for management of small pulmonary nodules detected on CT scans: a statement from the Fleischner Society. Radiology. 2005; 237(2):395–400. [PubMed: 16244247]

22. Schroeder T, Ruehm SG, Debatin JF, Ladd ME, Barkhausen J, Goehde SC. Detection of pulmonary nodules using a 2D HASTE MR sequence: comparison with MDCT. AJR Am J Roentgenol. 2005; 185(4):979–984. [PubMed: 16177419]
23. Regier M, Kandel S, Kaul MG, et al. Detection of small pulmonary nodules in high-field MR at 3 T: evaluation of different pulse sequences using porcine lung explants. Eur Radiol. 2007; 17(5): 1341–1351. [PubMed: 17013593]
24. Koyama H, Ohno Y, Kono A, et al. Quantitative and qualitative assessment of non-contrast-enhanced pulmonary MR imaging for management of pulmonary nodules in 161 subjects. Eur Radiol. 2008; 18(10):2120–2131. [PubMed: 18458913]
25. Yi CA, Jeon TY, Lee KS, et al. 3-T MRI: usefulness for evaluating primary lung cancer and small nodules in lobes not containing primary tumors. AJR Am J Roentgenol. 2007; 189(2):386–392. [PubMed: 17646465]
26. Biederer J, Schoene A, Freitag S, Reuter M, Heller M. Simulated pulmonary nodules implanted in a dedicated porcine chest phantom: sensitivity of MR imaging for detection. Radiology. 2003; 227(2):475–483. [PubMed: 12649421]
27. Eriksson P, Brattstrom D, Hesselius P, et al. Role of circulating cytokeratin fragments and angiogenic factors in NSCLC patients stage IIIa-IIIb receiving curatively intended treatment. Neoplasma. 2006; 53(4):285–290. [PubMed: 16830054]
28. Chen ZJ, Le HB, Zhang YK, Qian LY, Li WD. Microvessel density and expression of thrombospondin-1 in non-small cell lung cancer and their correlation with clinicopathological features. J Int Med Res. 2009; 37(2):551–556. [PubMed: 19383251]
29. Enatsu S, Iwasaki A, Shirakusa T, et al. Expression of hypoxia-inducible factor-1 alpha and its prognostic significance in small-sized adenocarcinomas of the lung. Eur J Cardiothorac Surg. 2006; 29(6):891–895. [PubMed: 16675263]
30. Yi CA, Lee KS, Kim EA, et al. Solitary pulmonary nodules: dynamic enhanced multi-detector row CT study and comparison with vascular endothelial growth factor and microvessel density. Radiology. 2004; 233(1):191–199. [PubMed: 15304661]
31. Li Y, Yang ZG, Chen TW, Chen HJ, Sun JY, Lu YR. Peripheral lung carcinoma: correlation of angiogenesis and first-pass perfusion parameters of 64-detector row CT. Lung Cancer. 2008; 61(1):44–53. [PubMed: 18055062]
32. Kusumoto M, Kono M, Adachi S, et al. Gadopentetate-dimeglumine-enhanced magnetic resonance imaging for lung nodules. Differentiation of lung cancer and tuberculoma Invest Radiol. 1994; 29(Suppl 2):S255–256.
33. Guckel C, Schnabel K, Deimling M, Steinbrich W. Solitary pulmonary nodules: MR evaluation of enhancement patterns with contrast-enhanced dynamic snapshot gradient-echo imaging. Radiology. 1996; 200(3):681–686. [PubMed: 8756914]
34. Ohno Y, Hatabu H, Takenaka D, Adachi S, Kono M, Sugimura K. Solitary pulmonary nodules: potential role of dynamic MR imaging in management initial experience. Radiology. 2002; 224(2): 503–511. [PubMed: 12147849]
35. Fujimoto K, Abe T, Muller NL, et al. Small peripheral pulmonary carcinomas evaluated with dynamic MR imaging: correlation with tumor vascularity and prognosis. Radiology. 2003; 227(3): 786–793. [PubMed: 12714678]
36. Ohno Y, Hatabu H, Takenaka D, et al. Dynamic MR imaging: value of differentiating subtypes of peripheral small adenocarcinoma of the lung. Eur J Radiol. 2004; 52(2):144–150. [PubMed: 15489071]
37. Schaefer JF, Vollmar J, Schick F, et al. Solitary pulmonary nodules: dynamic contrast-enhanced MR imaging--perfusion differences in malignant and benign lesions. Radiology. 2004; 232(2): 544–553. [PubMed: 15215548]
38. Schaefer JF, Schneider V, Vollmar J, et al. Solitary pulmonary nodules: association between signal characteristics in dynamic contrast enhanced MRI and tumor angiogenesis. Lung Cancer. 2006; 53(1):39–49. [PubMed: 16690161]
39. Kono R, Fujimoto K, Terasaki H, et al. Dynamic MRI of solitary pulmonary nodules: comparison of enhancement patterns of malignant and benign small peripheral lung lesions. AJR Am J Roentgenol. 2007; 188(1):26–36. [PubMed: 17179342]

40. Ohno Y, Koyama H, Takenaka D, et al. Dynamic MRI, dynamic multidetector-row computed tomography (MDCT), and coregistered 2-[fluorine-18]-fluoro-2-deoxy-D-glucose-positron emission tomography (FDG-PET)/CT: comparative study of capability for management of pulmonary nodules. J Magn Reson Imaging. 2008; 27(6):1284–1295. [PubMed: 18504748]
41. Sakai F, Sone S, Maruyama A, et al. Thin-rim enhancement in Gd-DTPA-enhanced magnetic resonance images of tuberculoma: a new finding of potential differential diagnostic importance. J Thorac Imaging. 1992; 7(3):64–69. [PubMed: 1501268]
42. Chung MH, Lee HG, Kwon SS, Park SH. MR imaging of solitary pulmonary lesion: emphasis on tuberculomas and comparison with tumors. J Magn Reson Imaging. 2000; 11(6):629–637. [PubMed: 10862062]
43. Gaeta M, Minutoli F, Ascenti G, et al. MR white lung sign: incidence and significance in pulmonary consolidations. J Comput Assist Tomogr. 2001; 25(6):890–896. [PubMed: 11711801]
44. Gaeta M, Vinci S, Minutoli F, et al. CT and MRI findings of mucin-containing tumors and pseudotumors of the thorax: pictorial review. Eur Radiol. 2002; 12(1):181–189. [PubMed: 11868096]
45. Sakai F, Sone S, Kiyono K, et al. MR of pulmonary hamartoma: pathologic correlation. J Thorac Imaging. 1994; 9(1):51–55. [PubMed: 8114166]
46. Fujimoto K, Meno S, Nishimura H, Hayabuchi N, Hayashi A. Aspergilloma within cavitary lung cancer: MR imaging findings. AJR Am J Roentgenol. 1994; 163(3):565–567. [PubMed: 8079845]
47. Blum U, Windfuhr M, Buitrago-Tellez C, Sigmund G, Herbst EW, Langer M. Invasive pulmonary aspergillosis. MRI, CT, and plain radiographic findings and their contribution for early diagnosis. Chest. 1994; 106(4):1156–1161. [PubMed: 7924489]
48. Satoh S, Kitazume Y, Ohdama S, Kimula Y, Taura S, Endo Y. Can malignant and benign pulmonary nodules be differentiated with diffusion-weighted MRI? AJR Am J Roentgenol. 2008; 191(2):464–470. [PubMed: 18647918]
49. Uto T, Takehara Y, Nakamura Y, et al. Higher sensitivity and specificity for diffusion-weighted imaging of malignant lung lesions without apparent diffusion coefficient quantification. Radiology. 2009; 252(1):247–254. [PubMed: 19420317]
50. Koyama H, Ohno Y, Aoyama N, et al. Comparison of STIR turbo SE imaging and diffusion-weighted imaging of the lung: capability for detection and subtype classification of pulmonary adenocarcinomas. Eur Radiol. 2010; 20(4):790–800. [PubMed: 19763578]
51. Feuerstein IM, Jicha DL, Pass HI, et al. Pulmonary metastases: MR imaging with surgical correlation--a prospective study. Radiology. 1992; 182(1):123–129. [PubMed: 1727274]
52. Kono M, Adachi S, Kusumoto M, Sakai E. Clinical utility of Gd-DTPA-enhanced magnetic resonance imaging in lung cancer. J Thorac Imaging. 1993; 8(1):18–26. [PubMed: 8418316]
53. Chiles C, Sherrier RH. Analysis of the solitary pulmonary nodule by means of digital techniques. J Thorac Imaging. 1990; 5(1):55–60. [PubMed: 2299703]
54. Chae EJ, Song JW, Seo JB, Krauss B, Jang YM, Song KS. Clinical utility of dual-energy CT in the evaluation of solitary pulmonary nodules: initial experience. Radiology. 2008; 249(2):671–681. [PubMed: 18796658]
55. Uemura M, Miyagawa M, Yasuhara Y, et al. Clinical evaluation of pulmonary nodules with dual-exposure dual-energy subtraction chest radiography. Radiat Med. 2005; 23(6):391–397. [PubMed: 16389980]
56. Ide K, Mogami H, Murakami T, Yasuhara Y, Miyagawa M, Mochizuki T. Detection of lung cancer using single-exposure dual-energy subtraction chest radiography. Radiat Med. 2007; 25(5):195–201. [PubMed: 17581707]
57. Eibel R, Turk TR, Kulinna C, Herrmann K, Reiser MF. Multidetector-row CT of the lungs: Multiplanar reconstructions and maximum intensity projections for the detection of pulmonary nodules. Fortschr Rontgenstr. 2001; 173(9):815–821.
58. Wang XH, Durick JE, Lu A, et al. Characterization of radiologists' search strategies for lung nodule detection: slice-based versus volumetric displays. J Digit Imaging. 2008; 21(Suppl 1):S39–49. [PubMed: 17874330]

59. Castellani U, Cristani M, Combi C, Murino V, Sbarbati A, Marzola P. Visual MRI: merging information visualization and non-parametric clustering techniques for MRI dataset analysis. Artif Intell Med. 2008; 44(3):183–199. [PubMed: 18775655]
60. Sakai S, Soeda H, Takahashi N, et al. Computer-aided nodule detection on digital chest radiography: validation test on consecutive T1 cases of resectable lung cancer. J Digit Imaging. 2006; 19(4):376–382. [PubMed: 16763934]
61. Awai K, Murao K, Ozawa A, et al. Pulmonary Nodules at Chest CT: Effect of computer-aided diagnosis on radiologists' detection performance. Radiology. 2004; 230(2):347–352. [PubMed: 14752180]
62. Wormans D, Beyer F, Diederich S, Ludwig K, Heindel W. Diagnositc performance of a commercially available computer-aided diagnosis system for automatic detection of pulmonary nodules: comparison with single and double reading. Fortschr Rontgenstr. 2004; 176:953–958.
63. Ikeda K, Awai K, Mori T, Kawanaka K, Yamashita Y, Nomori H. Differential diagnosis of ground-glass opacity nodules: CT number analysis by three-dimensional computerized quantification. Chest. 2007; 132(3):984–990. [PubMed: 17573486]
64. McNitt-Gray MF, Hart EM, Wyckoff N, Sayre JW, Goldin JG, Aberle DR. A pattern classification approach to characterizing solitary pulmonary nodules imaged on high resolution CT: preliminary results. Med Phys. 1999; 26(6):880–888. [PubMed: 10436888]
65. Shah SK, McNitt-Gray MF, Rogers SR, et al. Computer aided characterization of the solitary pulmonary nodule using volumetric and contrast enhancement features. Acad Radiol. 2005; 12(10):1310–1319. [PubMed: 16179208]
66. Nie Y, Li Q, Li F, Pu Y, Appelbaum D, Doi K. Integrating PET and CT information to improve diagnostic accuracy for lung nodules: A semiautomatic computer-aided method. J Nucl Med. 2006; 47(7):1075–1080. [PubMed: 16818939]
67. Armato SG 3rd, Roberts RY, Kocherginsky M, et al. Assessment of radiologist performance in the detection of lung nodules: dependence on the definition of “truth”. Acad Radiol. 2009; 16(1):28–38. [PubMed: 19064209]
68. Jirapatnakul AC, Fotin SV, Reeves AP, Biancardi AM, Yankelevitz DF, Henschke CI. Automated nodule location and size estimation using a multi-scale Laplacian of Gaussian filtering approach. Conf Proc IEEE Eng Med Biol Soc. 2009; 2009:1028–1031. [PubMed: 19964946]
69. Diciotti S, Lombardo S, Coppini G, Grassi L, Falchini M, Mascalchi M. The LoG characteristic scale: a consistent measurement of lung nodule size in CT imaging. IEEE Trans Med Imaging. 2010; 29(2):397–409. [PubMed: 20129846]
70. Knoss N, Hoffmann B, Fabel M, et al. Lung nodule assessment in computed tomography: precision of attenuation measurement based on computer-aided volumetry. Rofo. 2009; 181(12):1151–1156. [PubMed: 19859860]
71. Bolte H, Riedel C, Jahnke T, et al. Reproducibility of computer-aided volumetry of artificial small pulmonary nodules in ex vivo porcine lungs. Invest Radiol. 2006; 41(1):28–35. [PubMed: 16355037]
72. Bolte H, Jahnke T, Schafer FK, et al. Interobserver-variability of lung nodule volumetry considering different segmentation algorithms and observer training levels. Eur J Radiol. 2007; 64(2):285–295. [PubMed: 17433595]
73. Fink C, Puderbach M, Biederer J, et al. Lung MRI at 1.5 and 3 Tesla: observer preference study and lesion contrast using five different pulse sequences. Invest Radiol. 2007; 42(6):377–383. [PubMed: 17507808]
74. McNitt-Gray MF, Armato SG 3rd, Meyer CR, et al. The Lung Image Database Consortium (LIDC) data collection process for nodule detection and annotation. Acad Radiol. 2007; 14(12):1464–1474. [PubMed: 18035276]
75. Helferty JP, Sherbondy AJ, Kiraly AP, Higgins WE. Computer-based System for the Virtual-Endoscopic Guidance of Bronchoscopy. Comput Vis Image Underst. 2007; 108(1-2):171–187. [PubMed: 18978928]
76. Colt HG, Crawford SW, Galbraith O 3rd. Virtual reality bronchoscopy simulation: a revolution in procedural training. Chest. 2001; 120(4):1333–1339. [PubMed: 11591579]

77. Merritt SA, Gibbs JD, Yu KC, et al. Image-guided bronchoscopy for peripheral lung lesions: a phantom study. Chest. 2008; 134(5):1017–1026. [PubMed: 18583513]

78. McLennan G, Ferguson JS, Thomas K, Delsing AS, Cook-Granroth J, Hoffman EA. The use of MDCT-based computer-aided pathway finding for mediastinal and perihilar lymph node biopsy: a randomized controlled prospective trial. Respiration. 2007; 74(4):423–431. [PubMed: 17641484]

79. Suter MJ, Reinhardt JM, McLennan G. Integrated CT/bronchoscopy in the central airways: preliminary results. Acad Radiol. 2008; 15(6):786–798. [PubMed: 18486014]

80. Englmeier KH, Seemann MD. Multimodal virtual bronchoscopy using PET/CT images. Comput Aided Surg. 2008; 13(2):106–113. [PubMed: 18317959]

81. Herth FJ, Ernst A. Innovative bronchoscopic diagnostic techniques: endobronchial ultrasound and electromagnetic navigation. Curr Opin Pulm Med. 2005; 11(4):278–281. [PubMed: 15928491]

82. Schwarz Y, Mehta AC, Ernst A, et al. Electromagnetic navigation during flexible bronchoscopy. Respiration. 2003; 70(5):516–522. [PubMed: 14665778]

83. Lamprecht B, Porsch P, Pirich C, Studnicka M. Electromagnetic navigation bronchoscopy in combination with PET-CT and rapid on-site cytopathologic examination for diagnosis of peripheral lung lesions. Lung. 2009; 187(1):55–59. [PubMed: 18836886]

84. Becker HD, Herth F, Ernst A, Schwarz Y. Bronchoscopic biopsy of peripheral lung lesions under electromagnetic guidance: a pilot study. Journal of Bronchology. 2005; 12(1):9–13.

85. Priola AM, Priola SM, Cataldi A, et al. CT-guided percutaneous transthoracic biopsy in the diagnosis of mediastinal masses: evaluation of 73 procedures. Radiol Med. 2008; 113(1):3–15. [PubMed: 18338123]

86. Chan R, He Y, Haque A, Zwischenberger J. Computed tomographic-pathologic correlation of gross tumor volume and clinical target volume in non-small cell lung cancer: a pilot experience. Arch Pathol Lab Med. 2001; 125(11):1469–1472. [PubMed: 11698004]

87. Awaya H, Matsumoto T, Honjo K, Miura G, Emoto T, Matsunaga N. A preliminary study of discrimination among the components of small pulmonary nodules by MR imaging: correlation between MR images and histologic appearance. Radiat Med. 2000; 18(1):29–38. [PubMed: 10852653]

88. de Ryk J, Namati E, Thiesse J, McLennan G. New imaging approaches for understanding lung cancer response to treatment. Clin Pharmacol Ther. 2008; 84(4):517–522. [PubMed: 18769370]

89. Sieren JC, Weydert J, Namati E, et al. A process model for direct correlation between computed tomography and histopathology - application in lung cancer. Academic Radiology. 2010; 17(2): 169–180. [PubMed: 19926496]

90. Sieren JC, Weydert J, Bell A, et al. An Automated Segmentation Approach for Highlighting the Histological Complexity of Human Lung Cancer. Ann Biomed Eng. 2010

91. Namati E, De Ryk J, Thiesse J, Towfic Z, Hoffman E, McLennan G. Large image microscope array for the compilation of multimodality whole organ image databases. Anat Rec (Hoboken). 2007; 290(11):1377–1387. [PubMed: 17853414]

92. Sobin, L.; Gospodarowicz, M.; Wittekind, C. TNM Classification of Malignant Tumors. 7th. New York: Wiley-Liss; 2009. p. 136-147.

93. Webb WR, Gatsonis C, Zerhouni EA, et al. CT and MR imaging in staging non-small cell bronchogenic carcinoma: report of the Radiologic Diagnostic Oncology Group. Radiology. 1991; 178(3):705–713. [PubMed: 1847239]

94. Quint LE, Francis IR. Radiologic staging of lung cancer. J Thorac Imaging. 1999; 14(4):235–246. [PubMed: 10524804]

95. Herman SJ, Winton TL, Weisbrod GL, Towers MJ, Mentzer SJ. Mediastinal invasion by bronchogenic carcinoma: CT signs. Radiology. 1994; 190(3):841–846. [PubMed: 8115637]

96. Glazer HS, Kaiser LR, Anderson DJ, et al. Indeterminate mediastinal invasion in bronchogenic carcinoma: CT evaluation. Radiology. 1989; 173(1):37–42. [PubMed: 2781028]

97. White PG, Adams H, Crane MD, Butchart EG. Preoperative staging of carcinoma of the bronchus: can computed tomographic scanning reliably identify stage III tumours? Thorax. 1994; 49(10): 951–957. [PubMed: 7974310]

98. Takahashi M, Shimoyama K, Murata K, et al. Hilar and mediastinal invasion of bronchogenic carcinoma: evaluation by thin-section electron-beam computed tomography. J Thorac Imaging. 1997; 12(3):195–199. [PubMed: 9249677]

99. Yi CA, Shin KM, Lee KS, et al. Non-small cell lung cancer staging: efficacy comparison of integrated PET/CT versus 3.0-T whole-body MR imaging. Radiology. 2008; 248(2):632–642. [PubMed: 18552311]

100. White CS. MR evaluation of the pericardium and cardiac malignancies. Magn Reson Imaging Clin N Am. 1996; 4(2):237–251. [PubMed: 8724564]

101. Wong J, Haramati LB, Rozenshtein A, Yanez M, Austin JH. Non-small-cell lung cancer: practice patterns of extrathoracic imaging. Acad Radiol. 1999; 6(4):211–215. [PubMed: 10894078]

102. Takahashi K, Furuse M, Hanaoka H, et al. Pulmonary vein and left atrial invasion by lung cancer: assessment by breath-hold gadolinium-enhanced three-dimensional MR angiography. J Comput Assist Tomogr. 2000; 24(4):557–561. [PubMed: 10966186]

103. Ohno Y, Adachi S, Motoyama A, et al. Multiphase ECG-triggered 3D contrast-enhanced MR angiography: utility for evaluation of hilar and mediastinal invasion of bronchogenic carcinoma. J Magn Reson Imaging. 2001; 13(2):215–224. [PubMed: 11169827]

104. Higashino T, Ohno Y, Takenaka D, et al. Thin-section multiplanar reformats from multidetector-row CT data: utility for assessment of regional tumor extent in non-small cell lung cancer. Eur J Radiol. 2005; 56(1):48–55. [PubMed: 16168264]

105. Magdeleinat P, Alifano M, Benbrahem C, et al. Surgical treatment of lung cancer invading the chest wall: results and prognostic factors. Ann Thorac Surg. 2001; 71(4):1094–1099. [PubMed: 11308142]

106. Yokoi K, Mori K, Miyazawa N, Saito Y, Okuyama A, Sasagawa M. Tumor invasion of the chest wall and mediastinum in lung cancer: evaluation with pneumothorax CT. Radiology. 1991; 181(1):147–152. [PubMed: 1887024]

107. Murata K, Takahashi M, Mori M, et al. Chest wall and mediastinal invasion by lung cancer: evaluation with multisection expiratory dynamic CT. Radiology. 1994; 191(1):251–255. [PubMed: 8134583]

108. Rapoport S, Blair DN, McCarthy SM, Desser TS, Hammers LW, Sostman HD. Brachial plexus: correlation of MR imaging with CT and pathologic findings. Radiology. 1988; 167(1):161–165. [PubMed: 3347719]

109. Heelan RT, Demas BE, Caravelli JF, et al. Superior sulcus tumors: CT and MR imaging. Radiology. 1989; 170(3 Pt 1):637–641. [PubMed: 2916014]

110. Padovani B, Mouroux J, Seksik L, et al. Chest wall invasion by bronchogenic carcinoma: evaluation with MR imaging. Radiology. 1993; 187(1):33–38. [PubMed: 8451432]

111. Bonomo L, Ciccotosto C, Guidotti A, Storto ML. Lung cancer staging: the role of computed tomography and magnetic resonance imaging. Eur J Radiol. 1996; 23(1):35–45. [PubMed: 8872072]

112. Freundlich IM, Chasen MH, Varma DG. Magnetic resonance imaging of pulmonary apical tumors. J Thorac Imaging. 1996; 11(3):210–222. [PubMed: 8784734]

113. Sakai S, Murayama S, Murakami J, Hashiguchi N, Masuda K. Bronchogenic carcinoma invasion of the chest wall: evaluation with dynamic cine MRI during breathing. J Comput Assist Tomogr. 1997; 21(4):595–600. [PubMed: 9216765]

114. Watanabe H, Okada M, Kaji Y, et al. New response evaluation criteria in solid tumours-revised RECIST guideline (version 1.1). Gan To Kagaku Ryoho. 2009; 36(13):2495–2501. [PubMed: 20009446]

115. Rasmussen F. RECIST and targeted therapy. Acta Radiol. 2009; 50(8):835–836. [PubMed: 19863421]

116. Bourgouin PM, McLoud TC, Fitzgibbon JF, et al. Differentiation of bronchogenic carcinoma from postobstructive pneumonitis by magnetic resonance imaging: histopathologic correlation. J Thorac Imaging. 1991; 6(2):22–27. [PubMed: 1856898]

117. Ohno Y, Adachi S, Kono M, Kusumoto M, Motoyama A, Sugimura K. Predicting the prognosis of non-small cell lung cancer patient treated with conservative therapy using contrast-enhanced MR imaging. Eur Radiol. 2000; 10(11):1770–1781. [PubMed: 11097405]

118. Dillemans B, Deneffe G, Verschakelen J, Decramer M. Value of computed tomography and mediastinoscopy in preoperative evaluation of mediastinal nodes in non-small cell lung cancer. A study of 569 patients. Eur J Cardiothorac Surg. 1994; 8(1):37–42. [PubMed: 8136168]

119. McLoud TC, Bourgouin PM, Greenberg RW, et al. Bronchogenic carcinoma: analysis of staging in the mediastinum with CT by correlative lymph node mapping and sampling. Radiology. 1992; 182(2):319–323. [PubMed: 1732943]

120. Webb WR, Sarin M, Zerhouni EA, Heelan RT, Glazer GM, Gatsonis C. Interobserver variability in CT and MR staging of lung cancer. J Comput Assist Tomogr. 1993; 17(6):841–846. [PubMed: 8227566]

121. Wahl RL, Quint LE, Greenough RL, Meyer CR, White RI, Orringer MB. Staging of mediastinal non-small cell lung cancer with FDG PET, CT, and fusion images: preliminary prospective evaluation. Radiology. 1994; 191(2):371–377. [PubMed: 8153308]

122. Patz EF Jr, Lowe VJ, Goodman PC, Herndon J. Thoracic nodal staging with PET imaging with 18FDG in patients with bronchogenic carcinoma. Chest. 1995; 108(6):1617–1621. [PubMed: 7497771]

123. Higashi K, Nishikawa T, Seki H, et al. Comparison of fluorine-18-FDG PET and thallium-201 SPECT in evaluation of lung cancer. J Nucl Med. 1998; 39(1):9–15. [PubMed: 9443730]

124. Gupta NC, Graeber GM, Bishop HA. Comparative efficacy of positron emission tomography with fluorodeoxyglucose in evaluation of small (<1 cm), intermediate (1 to 3 cm), and large (>3 cm) lymph node lesions. Chest. 2000; 117(3):773–778. [PubMed: 10713005]

125. Boiselle PM, Patz EF Jr, Vining DJ, Weissleder R, Shepard JA, McLoud TC. Imaging of mediastinal lymph nodes: CT, MR, and FDG PET. Radiographics. 1998; 18(5):1061–1069. [PubMed: 9747607]

126. Takenaka D, Ohno Y, Hatabu H, et al. Differentiation of metastatic versus non-metastatic mediastinal lymph nodes in patients with non-small cell lung cancer using respiratory-triggered short inversion time inversion recovery (STIR) turbo spin-echo MR imaging. Eur J Radiol. 2002; 44(3):216–224. [PubMed: 12468071]

127. Ohno Y, Hatabu H, Takenaka D, et al. Metastases in mediastinal and hilar lymph nodes in patients with non-small cell lung cancer: quantitative and qualitative assessment with STIR turbo spin-echo MR imaging. Radiology. 2004; 231(3):872–879. [PubMed: 15163823]

128. Ohno Y, Koyama H, Nogami M, et al. STIR turbo SE MR imaging vs. coregistered FDG-PET/CT: quantitative and qualitative assessment of N-stage in non-small-cell lung cancer patients. J Magn Reson Imaging. 2007; 26(4):1071–1080. [PubMed: 17896365]

129. Pannu HK, Wang KP, Borman TL, Bluemke DA. MR imaging of mediastinal lymph nodes: evaluation using a superparamagnetic contrast agent. J Magn Reson Imaging. 2000; 12(6):899–904. [PubMed: 11105028]

130. Kernstine KH, Stanford W, Mullan BF, et al. PET, CT, and MRI with Combidex for mediastinal staging in non-small cell lung carcinoma. Ann Thorac Surg. 1999; 68(3):1022–1028. [PubMed: 10510001]

131. Nguyen BC, Stanford W, Thompson BH, et al. Multicenter clinical trial of ultrasmall superparamagnetic iron oxide in the evaluation of mediastinal lymph nodes in patients with primary lung carcinoma. J Magn Reson Imaging. 1999; 10(3):468–473. [PubMed: 10508310]

132. Yeh DW, Lee KS, Han J, et al. Mediastinal nodes in patients with non-small cell lung cancer: MRI findings with PET/CT and pathologic correlation. AJR Am J Roentgenol. 2009; 193(3):813–821. [PubMed: 19696297]

133. Hasegawa I, Boiselle PM, Kuwabara K, Sawafuji M, Sugiura H. Mediastinal lymph nodes in patients with non-small cell lung cancer: preliminary experience with diffusion-weighted MR imaging. J Thorac Imaging. 2008; 23(3):157–161. [PubMed: 18728541]

134. Quint LE, Tummala S, Brisson LJ, et al. Distribution of distant metastases from newly diagnosed non-small cell lung cancer. Ann Thorac Surg. 1996; 62(1):246–250. [PubMed: 8678651]

135. Pantel K, Izbicki J, Passlick B, et al. Frequency and prognostic significance of isolated tumour cells in bone marrow of patients with non-small-cell lung cancer without overt metastases. Lancet. 1996; 347(9002):649–653. [PubMed: 8596379]

136. Silvestri GA, Gould MK, Margolis ML, et al. Noninvasive staging of non-small cell lung cancer: ACCP evidenced-based clinical practice guidelines (2nd edition). Chest. 2007; 132(3 Suppl): 178S–201S. [PubMed: 17873168]

137. van Tinteren H, Hoekstra OS, Smit EF, et al. Effectiveness of positron emission tomography in the preoperative assessment of patients with suspected non-small-cell lung cancer: the PLUS multicentre randomised trial. Lancet. 2002; 359(9315):1388–1393. [PubMed: 11978336]

138. Walker R, Kessar P, Blanchard R, et al. Turbo STIR magnetic resonance imaging as a whole-body screening tool for metastases in patients with breast carcinoma: preliminary clinical experience. J Magn Reson Imaging. 2000; 11(4):343–350. [PubMed: 10767062]

139. Antoch G, Vogt FM, Freudenberg LS, et al. Whole-body dual-modality PET/CT and whole-body MRI for tumor staging in oncology. Jama. 2003; 290(24):3199–3206. [PubMed: 14693872]

140. Lauenstein TC, Goehde SC, Herborn CU, et al. Whole-body MR imaging: evaluation of patients for metastases. Radiology. 2004; 233(1):139–148. [PubMed: 15317952]

141. Takahara T, Imai Y, Yamashita T, Yasuda S, Nasu S, Van Cauteren M. Diffusion weighted whole body imaging with background body signal suppression (DWIBS): technical improvement using free breathing, STIR and high resolution 3D display. Radiat Med. 2004; 22(4):275–282. [PubMed: 15468951]

142. Goehde SC, Hunold P, Vogt FM, et al. Full-body cardiovascular and tumor MRI for early detection of disease: feasibility and initial experience in 298 subjects. AJR Am J Roentgenol. 2005; 184(2):598–611. [PubMed: 15671386]

143. Schmidt GP, Haug AR, Schoenberg SO, Reiser MF. Whole-body MRI and PET-CT in the management of cancer patients. Eur Radiol. 2006; 16(6):1216–1225. [PubMed: 16538426]

144. Charles-Edwards EM, deSouza NM. Diffusion-weighted magnetic resonance imaging and its application to cancer. Cancer Imaging. 2006; 6:135–143. [PubMed: 17015238]

145. Ohno Y, Koyama H, Nogami M, et al. Whole-body MR imaging vs. FDG-PET: comparison of accuracy of M-stage diagnosis for lung cancer patients. J Magn Reson Imaging. 2007; 26(3): 498–509. [PubMed: 17729341]

146. Ohno Y, Koyama H, Onishi Y, et al. Non-small cell lung cancer: whole-body MR examination for M-stage assessment--utility for whole-body diffusion-weighted imaging compared with integrated FDG PET/CT. Radiology. 2008; 248(2):643–654. [PubMed: 18539889]

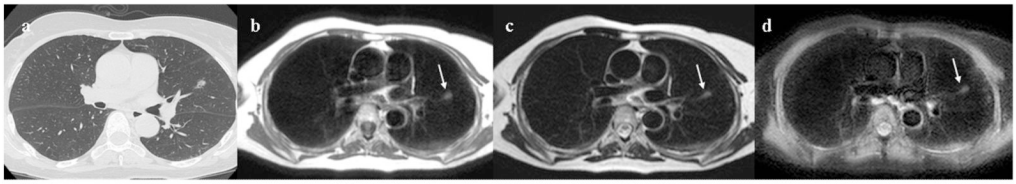

Figure 1. 71-year-old female with adenomatous hyperplasia in the left upper lobe

Thin-section CT indicates ground-glass attenuation (GGA) in the left upper lobe (Fig.1a). The diameter of this GGA is 8mm in diameter. Black-blood T1-weighted turbo spin-echo (SE) (Fig.1b), T2-weighted turbo SE (Fig.1c) and STIR turbo SE (Fig.1d) images show a nodule (arrow) as, respectively, low, intermediate and high signal intensity in the same lobe.

Figure 2. 76-year-old male with adenocarcinoma in the left upper lobe

Thin-section CT shows a cavitary nodule in the left upper lobe (Fig. 2a). The diameter of this nodule is 16mm in diameter. Black-blood T1-weighted turbo SE (Fig. 2b), T2-weighted turbo SE (Fig. 2c) and STIR turbo SE (Fig. 2d) images show nodule (arrow) as, respectively, low, intermediate and high signal intensity in the left upper lobe. Post-contrast enhanced black-blood T1-weighted turbo SE image (Fig. 2e) showed homogeneous enhancement of nodule.

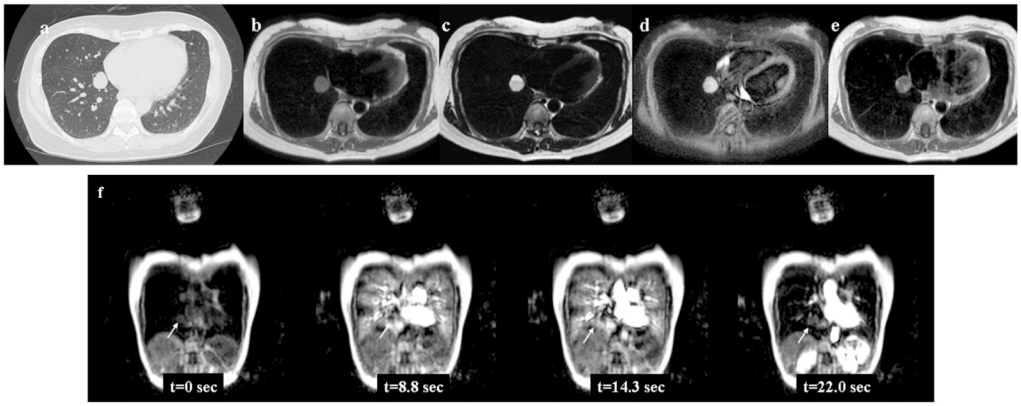

Figure 3. 48-year-old female with hamartoma in the right lower lobe

Thin-section CT with lung window setting (Fig. 3a) shows a solid nodule in the right lower lobe (Fig. 3a). The diameter of this nodule is 20 mm. Black-blood T1-weighted turbo SE (Fig. 3b), T2-weighted turbo SE (Fig. 3c) and STIR turbo SE (Fig. 3d) images show nodule (arrow) as, respectively, low, intermediate and high signal intensity in the right lower lobe. Post-contrast enhanced black-blood T1-weighted turbo SE image (Fig. 3e) showed heterogeneous enhancement of nodule. Dynamic MR imaging (Fig. 3f) with ultrafast-GRE technique (L to R: t=0.0 sec, t=8.8 sec, t=14.3 sec and t=22.0 sec) shows a slightly enhanced nodule in the right lower lung field. The nodule is gradually enhanced in the lung parenchymal phase (t=8.8 and 14.3 sec) and slightly enhanced in the systemic circulation phase (t= 22.0 sec) due to low blood supply.

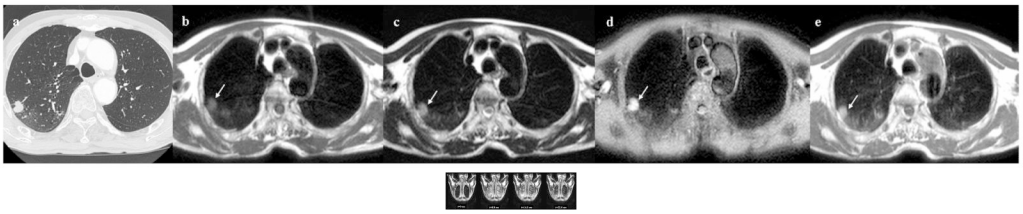

Figure 4. 76-year-old male with adenocarcinoma in the right upper lobe

Thin-section contrast-enhanced CT shows a solid nodule in the right upper lobe (Fig. 4a). The diameter of this nodule is 12mm. Black-blood T1-weighted turbo SE (Fig. 4b), T2-weighted turbo SE (Fig. 4c) and STIR turbo SE (Fig. 4d) images show nodule (arrow) as, respectively, low, intermediate and high signal intensity in the right upper lobe. Post-contrast enhanced black-blood T1-weighted turbo SE image (Fig. 4e) showed homogeneous enhancement of nodule. Dynamic MR imaging (Fig. 4f) with ultrafast-GRE technique (L to R: t=0.0 sec, t=8.8 sec, t=14.3 sec and t=22.0 sec) shows a markedly enhanced nodule in the right upper lung field. The nodule is enhanced in the lung parenchymal phase (t=8.8 and 14.3 sec) and the systemic circulation phase (t=22.0 sec) due to high blood supply.

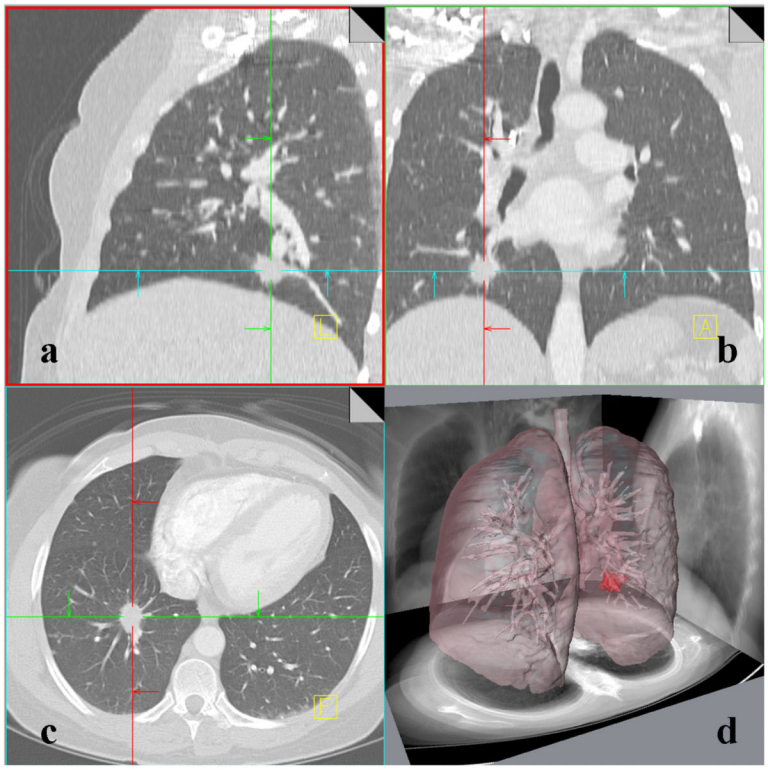

Figure 5. 51-year-old female with adenocarcinoma

A multi-detector computed tomography (MDCT) dataset displayed using the traditional three cross-sectional image planes: sagittal (Fig. 5a), coronal (Fig. 5b) and axial (Fig. 5c). A volumetric display created in AMIRA (Visage Imaging, Andover, MA, USA) clearly portrays the nodule shape and proximity to nearby structures in the lung such as airways within a single image (Fig. 5d).

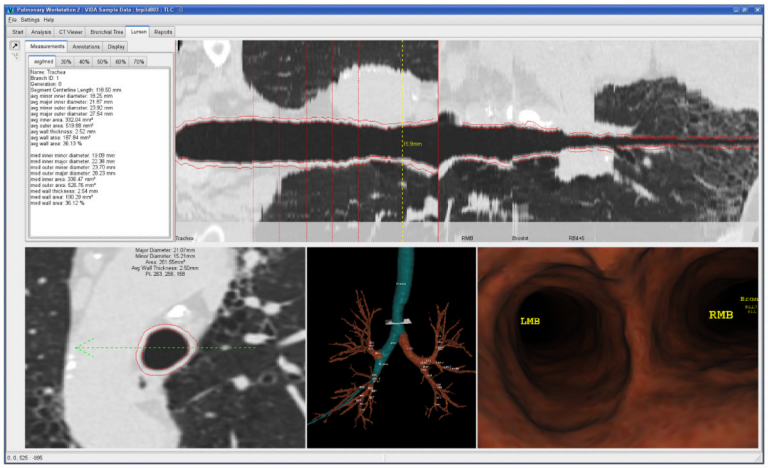

Figure 6. Virtual bronchoscopy guided biopsy of a peripheral pulmonary nodule

The planning of a virtual bronchoscopy path from the trachea to a peripheral airway is illustrated in a number of views, including; the straightened lumen view, the axial cross section with airway measurements, the 3D airway tree reconstruction with highlighted path and the virtual bronchoscopy fly-through with airway labels (Courtesy of VIDA diagnostics, Coralville, IA, USA).

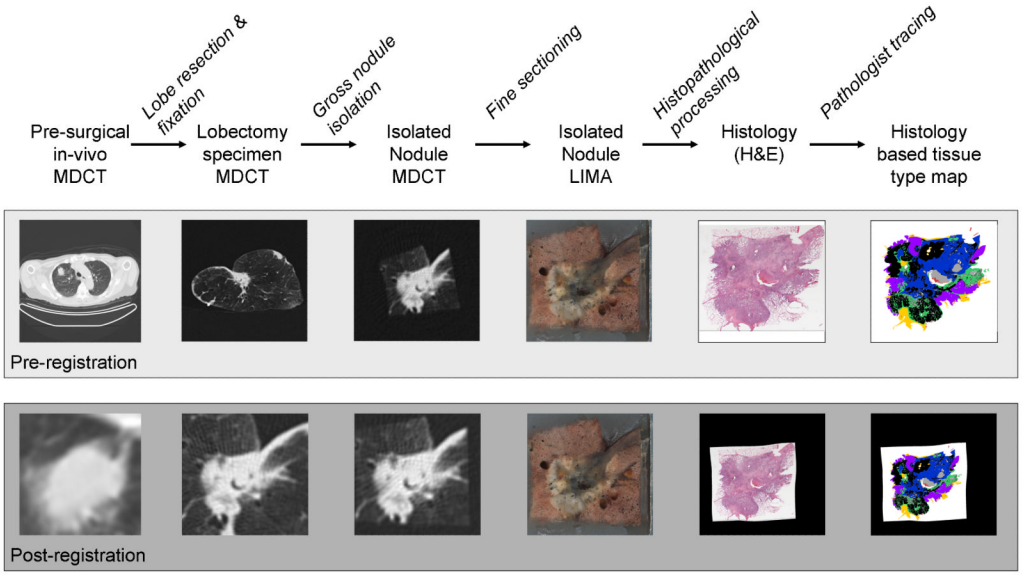

Figure 7. 79-year-old female with adenocarcinoma

A adenocarcinoma nodule was imaged prior to and following lobectomy resection, to produce a 3D, cross-registered, multimodal, multi-resolution dataset. The dataset contains density information from in-vivo multi-detector computed tomography (MDCT), MDCT of the fixed lobectomy specimen and MDCT of the isolated nodule. Color information is obtained from the purpose-built, macroscopic Large Image Microscope Array (LIMA). Information regarding the histological content of the nodule is gained from the digitized hematoxylin and eosin (H&E) histopathology slide which was utilized by a pathologist to create a color coded tissue type map. The tissue type map shows solid cancerous tumor (black), bronchioloalveolar tumor (purple), active fibrosis (green), inactive fibrosis (blue), necrosis (grey), blood (red) and normal tissues (yellow).

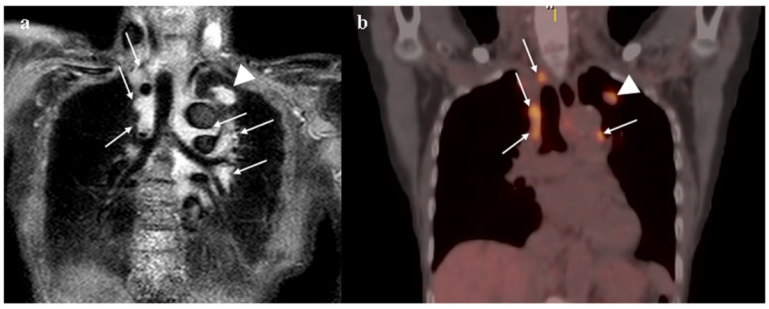

Figure 8. 76-year-old male with adenocarcinoma (N3)

Black-blood STIR turbo SE imaging on coronal plane (Fig. 5a) shows mediastinal and hilar lymph nodes (arrows) and primary lesion (arrow head) as high signal intensity, and suggests a diagnosis of N3. Black-blood STIR turbo SE imaging showed this case to be true-positive. Integrated FDG-PET/CT (Fig. 5b) demonstrates high uptake of FDG in the mediastinal and hilar lymph nodes (arrows) and primary lesion (arrow head). Both methods suggest a diagnosis of N3. This case was pathologically proven as N3 according to the results of biopsy.

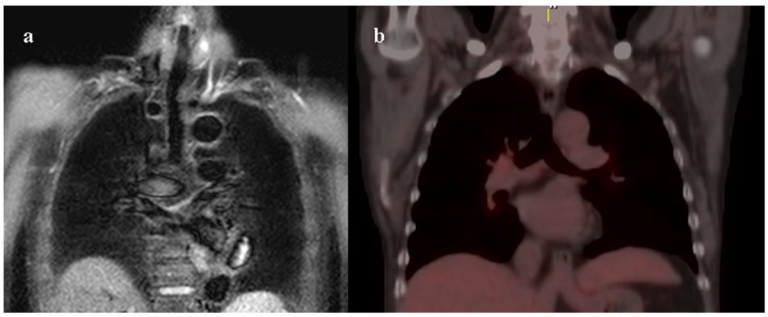

Figure 9. 77-year-old male with adenocarcinoma (N0)

Black-blood STIR turbo SE imaging on coronal plane (Fig. 5a) show no abnormal high intensities in the mediastinal and hilar lymph nodes. Integrated FDG-PET/CT (Fig. 6a) also demonstrates no abnormal uptake of FDG in the mediastinal and hilar lymph nodes. Both methods suggest a diagnosis of N0. This case was pathologically proven as N0 after surgical treatment.